Nuclear Materials and Energy 21 (2019) 100706

Contents lists available at ScienceDirect

Nuclear Materials and Energy

journal homepage: www.elsevier.com/locate/nme

Effects of U-Mo irradiation creep coefficient on the mesoscale mechanical behavior in U-Mo/Al monolithic fuel plates

Jian Xiaobin, Yan Feng, Kong Xiangzhe, Ding Shurong*

Institute of Mechanics and Computational Engineering, Department of Aeronautics and Astronautics, Fudan University, Shanghai 200433, China

ARTICLE INFO

Keywords:
Bubble volume fraction
Bubble pressure
Irradiation creep coefficient
Porous media
Mesoscale normal stress
Creep damage

ABSTRACT

The fuel foils in U-Mo/Al monolithic fuel plates will evolve into porous media owing to the formed gas bubbles. Three-dimensional finite element simulations are implemented for the thermo-mechanical behavior in U-Mo/Al monolithic fuel plates with different U-Mo irradiation creep coefficients, and the results of mesoscale normal stress, bubble volume fraction and bubble pressure in the fuel foil are obtained. In the simulations, the mechanistic fission gas swelling model is adopted, considering the dependence of external hydrostatic pressure. The mesoscale normal stress refers to the effective normal stress in the skeleton of porous fuel foil, which relates to the fuel fracture. The numerical results indicate that an irradiation creep coefficient of 2000×10^{-31} m^3/MPa can be identified for the current U-10Mo fuel foil, because the calculated fuel-foil thickness increments match well with the experimental data. The influences of U-Mo irradiation creep coefficient on its bubble volume fraction and pore pressure are significant in the vicinity of fuel foil edges and corners. The dangerous regions locate near the fuel foil corners, surrounding the points with maximum mesoscale normal stresses. The enlarged irradiation creep coefficient will result in stress relaxation on the whole, but the through-thickness creep strain components can be heavily magnified. When the irradiation creep coefficient increases from 10×10^{-31} m^3/MPa to 1000×10^{-31} m^3/MPa, the maximum mesoscale normal stresses will decrease from 58.04 MPa to 28.04 MPa, with a reduction of ~52%; while the corresponding through-thickness creep strain components increase by ~5%. With an increase of irradiation creep coefficient from 1000×10^{-31} m^3/MPa to 2000×10^{-31} m^3/MPa, the maximum mesoscale normal stresses increase by ~9%, and the corresponding through-thickness creep strain components increase by ~219%. The irradiation creep performance should be optimized and an extreme large creep coefficient is not a good choice, because the creep-induced damage might degrade the mesoscale strength of the fuel foil.

1. Introduction

U-Mo alloy has become a most potential fuel foil for monolithic fuel plates in research and test reactors, due to its high uranium density and good performances under irradiation conditions [1–3]. Laminated U-Mo/Al monolithic fuel plates are superior to dispersion fuel plates in some aspects, which can enhance the neutron flux of the reactors and avoid the chemical interaction of U-Mo with the structural materials to a great extent [4]. However, fracture was observed to occur in the U-Mo fuel foil close to the Zr diffusion layer in post-irradiation examination [4]. The fuel fracture mechanism and influencing factors should be captured, in order to further improve the service lifetime of monolithic fuel plates.

The key factors to affect the fracture behavior of fuel foil are irradiation swelling and irradiation creep. The former induces the mechanical interaction between the fuel foil and the cladding. Especially, irradiation swelling results from two contributions, namely fission solid swelling and fission gas swelling. The fission gas swelling is mainly attributed to the gas bubbles formed in the grain boundaries. The formed bubbles will make the fuel foil evolve into a porous structure, and the bubble volume fraction and bubble pressure will degrade the thermo-mechanical properties of U-Mo alloy [5–8]. Irradiation creep will relax and redistribute the stresses in the fuel foil, which tends to improve the safety of fuel foil. However, the creep-induced damage may weaken the strength of irradiated U-Mo skeleton, just like some other metal alloys [9–11]. It is a critical problem to optimize the irradiation creep performance for U-Mo fuel foil.

At present, a mesoscale normal stress model has been developed to evaluate the fracture behavior of U-Mo fuel foil [12], which can be used to obtain the effective normal stress in the skeleton of porous U-Mo fuel.

* Corresponding author.
E-mail address: dingshurong@fudan.edu.cn (S. Ding).

https://doi.org/10.1016/j.nme.2019.100706
Received 21 August 2019; Accepted 24 September 2019
Available online 26 September 2019

The mesoscale normal stresses depend on the bubble volume fraction, bubble pressure and bubble size [13,14], which are all related to fission gas swelling. There are two acceptable models to describe the fission gas swelling of U-Mo alloy, including the empirical formula and the mechanistic model. The empirical formula [15] is simple and only dependent on fission density; but it can't reflect the influence of many parameters, such as the temperature, the grain size, the fission rate and external hydrostatic pressure, etc.; moreover, the bubble size and bubble pressure are difficult to be derived from this model. The other fission gas swelling model is based on the mechanistic models for the fission gas diffusion behavior within the fuel grain, with the bubble nucleation mechanism and recrystallization theory involved [16,17]. This mechanistic fission gas swelling model considers the influences of intergranular gas atom resolution and external hydrostatic-pressure dependence of bubble radius, and the obtained swelling results agree well with the experimental data [18]. In addition, the models for bubble volume fraction, bubble pressure and bubble size have been proposed based on the mechanistic fission gas swelling [12]. Accordingly, the mesoscale normal stresses of porous fuel foil were developed and introduced to numerical simulation of the thermo-mechanical behavior in U-Mo/Al monolithic fuel plates [12].

An irradiation creep rate model linearly dependent on the fission rate and stress was developed for U-Mo alloys [19]. The irradiation creep coefficient of 500×10^{-31} m^3/MPa was recommended by Kim et al. [20] for U-10Mo, with the two-dimensional numerical results of fuel foil thickness increment compared with the experimental data. The numerical results were obtained with the empirical fission gas swelling model. The mechanical constitutive relation for the Al alloy was regarded as a simple one, without considering the thermal creep effect and the irradiation-dose dependence for the plastic model. In fact, the simulation results for the thickness increments of irradiated U-Mo fuel foil have a comprehensive relation with the models of fission gas swelling, irradiation creep, thermal expansion and the constitutive models for the Al cladding. If the mechanistic fission gas swelling model for fuel foil is adopted together with different constitutive models for the Al cladding, the identified irradiation creep coefficient may differ from the value of 500×10^{-31} m^3/MPa.

Considering that the creep performances for metallic fuels are closely related to their fabrication process, microstructure and chemical components [20–22], the creep coefficient for different U-Mo foils should be discrepant. In order to optimize the creep properties for U-Mo alloys, the effects of irradiation creep coefficient on the mesoscale mechanical behavior in the fuel foils of monolithic fuel plates should be analyzed.

Three-dimensional (3D) numerical studies have been performed for U-Mo/Al monolithic fuel plate with the mechanical swelling model for U-Mo foil, and the macroscale thermo-mechanical behavior was analyzed [23]. The creep coefficient for U-10Mo was identified with 3D numerical simulation, and the effects of U-Mo creep coefficient on the macroscale thermo-mechanical behavior in monolithic fuel plates are obtained [24], with the irradiation-dose dependent plastic model and thermal creep model involved in the constitutive relation for the cladding. However, the empirical formula model for fission gas swelling was used [24]. The effects of U-Mo irradiation creep coefficient on the mesoscale mechanical behavior in U-Mo/Al monolithic fuel plates have not been reported.

In this study, 3D finite element simulations are implemented with the irradiation dependent thermo-mechanical properties taken into account, especially using the mechanistic fission gas swelling model for fuel foil. The effects of U-Mo irradiation creep coefficient are investigated on the distribution and evolution of bubble volume fraction, the thickness increments, the through-thickness creep strain components, and mesoscale normal stress. This work can lay a foundation for optimization of U-Mo alloys.

2. Material properties and mesoscale normal stress model for porous fuels

2.1. Material properties

2.1.1. Material properties for U-Mo fuels

(1) Young's modulus and Poisson's ratio

The mechanical properties dependent on bubble volume fraction are adopted as [25]

$$E = E_0 \frac{(1-\phi)^2}{(1+(2-3\nu_0)\phi)}$$
$$\nu = \frac{4\nu_0 + 3\phi - 7\nu_0\phi}{4(1+2\phi-3\nu_0\phi)} \quad (1)$$

where, ϕ is the bubble volume fraction, E_0 and ν_0 are the Young's modulus and Poisson's ratio for as-fabricated U-Mo fuels, which are set as 85 GPa and 0.34 [20].

(2) Thermal conductivity

The thermal conductivity for un-irradiated U-Mo alloys can be expressed as [7,26]

$$k^0_{U-Mo} = (1-\sqrt{1-\chi_{Mo}})k_{Mo} + \sqrt{1-\chi_{Mo}}\{(1-\chi_{Mo})k_U + \chi_{Mo}k_{c,Mo}\} \quad (2)$$

$$k_U(T) = 21.73 + 1.591 \times 10^{-2}T + 5.907 \times 10^{-6}T^2 \quad (3)$$

$$k_{Mo}(T) = 150.0 - 4.0 \times 10^{-2}T \quad (4)$$

$$k_{c,Mo}(T) = -274.4 + 985.2\chi_{Mo} - 1.941 \times 10^3\chi^2_{Mo} + 3.640 \times 10^{-2}T + 7.365 \times 10^{-5}T^2 + 5.793 \times 10^{-2}\chi_{Mo}T \quad (5)$$

where, k^0_{U-Mo} is in Wm^{-1} K^{-1}; χ_{Mo} is Mo concentration in weight percent, with a value of 0.1 for U-10Mo; T is the temperature in K.

The thermal conductivity for irradiated U-Mo fuels is given as [7]

$$k_{U-Mo} = \frac{1}{4}[D + \sqrt{D^2 + 8k^0_{U-Mo}k_g}] \quad (6)$$

$$D = (2-3\phi)k^0_{U-Mo} + (3\phi-1)k_g \quad (7)$$

$$k_g = 0.1(8.247 \times 10^{-5}T^{0.8363}) + 0.9(4.351 \times 10^{-5}T^{0.8616}) \quad (8)$$

(3) The thermal expansion coefficient

The thermal expansion coefficient α in K^{-1} is related to temperature [27], which can be expressed as

$$\alpha = \begin{cases} (3 \times 10^{-5}T^2 - 1.698 \times 10^{-2}T + 13.9497) \times 10^{-6} & T \le 673K \\ (-5 \times 10^{-6}T^2 + 1.023 \times 10^{-2}T + 11.4709) \times 10^{-6} & T > 673K \end{cases} \quad (9)$$

(4) The irradiation swelling

The recrystallization occurs when the fission density excesses the critical value. The critical fission density depends on the fission rate $\dot{f}$ [16], expressed as

$$F_{dx} = 6 \times 10^{24}(\dot{f})^{2/15} \quad (10)$$

The volume fraction V_r of recrystallized area can be used to describe the recrystallization process, given as

$$V_r = 1 - \left[1 - \frac{16\gamma B_2(F_d - F_{dx})}{r_{gr0}}\sqrt{\frac{(1-\nu/2)(1-\nu)}{2\pi}}\right]^3 \quad (11)$$

where, γ is the surface tension with a value of 1 N/m [16]; ν is the Poisson's ratio; B_2 is a calculation parameter, which is set as

1.0×10^{-34} m^5/N [16]; F_d depicts the current fission density, and the initial grain radius r_{gr0} is set as 3.5×10^{-6} m [16].

The total irradiation swelling involves the fission gas swelling and the fission solid swelling. The fission solid swelling has a linear relation with the fission density [15], given as

$$SW_s = 4.0 \times 10^{-29} \cdot F_d \tag{12}$$

The fission gas swelling is expressed with a two-stage model. Before recrystallization, it is composed of the contributions from intragranular bubbles and intergranular bubbles. After recrystallization initiation, the fission gas swelling is a homogenized value of those for the un-recrystallized and recrystallized areas. The fission gas swelling for the recrystallized area is considered to only stem from intergranular bubbles due to the depletion of fission gas atoms within the fine grains. So, the fission gas swelling is expressed as

$$SW_{gas} = \begin{cases} \left(\frac{\Delta V_{intra}}{V}\right)\Big|_{r_{gr0}} + \left(\frac{\Delta V_{inter}}{V}\right)\Big|_{r_{gr0}} & F_d \le F_{dx} \\ (1 - V_r)\left[\left(\frac{\Delta V_{intra}}{V}\right)\Big|_{r_{gr}} + \left(\frac{\Delta V_{inter}}{V}\right)\Big|_{r_{gr}}\right] + V_r & F_d > F_{dx} \\ \left(\frac{\Delta V_{inter}}{V}\right)\Big|_{r_{grx}} & \end{cases} \tag{13}$$

It is noted that the fission gas swelling model adopted in this study is a mechanistic model, where the contributions from the intragranular bubbles and intergranular bubbles are calculated with the surface concentration of the fission gas atoms in the grain boundaries. More details can be found in Refs. [16,28]. Especially, the intergranular bubble radius is considered to be affected by the external hydrostatic pressure [28].

(5) The irradiation creep

The creep rate model is described as

$$\frac{d\varepsilon^{cr}}{dt} = A\sigma\dot{f} \tag{14}$$

where $\frac{d\varepsilon^{cr}}{dt}$ is the equivalent creep rate; A denotes the irradiation creep coefficient. In this study, different creep coefficients of 10, 100, 500, 1000 and 2000×10^{-31} m^3/MPa are adopted to investigate their effects on the in-pile mesoscale mechanical behavior in the porous U- Mo foil of monolithic fuel plates.

2.1.2. Material properties for Al 6061 under irradiation conditions

(1) The elastic-plastic property

A Young's modulus of 66 GPa and Poisson's ratio of 0.34 are taken from Ref. [20].

The plastic behavior of Al 6061 will be affected by the temperature and fast neutron fluence [29]. The relationship between true stress and true strain is fitted with the experiment data [29], given as [24]

$$\sigma = k(T)g(\varphi)\varepsilon^{0.06281} \tag{15}$$

$$k(T) = 2.008 \times (130.54 + 2.425T - 1.949\times10^{-2}T^2 + 6.2048 \times 10^{-5}T^3 - 6.6204 \times 10^{-8}T^4)^{0.93719} \quad 300\text{K} \le T \le 490\text{K} \tag{16}$$

$$g(\varphi) = \begin{cases} 1 & \varphi < 2.4 \\ \left[0.195 \times \log\left(\frac{\varphi}{2.4}\right) + 1\right]^{0..93719} & \varphi \ge 2.4 \end{cases} \tag{17}$$

where φ denotes the fast neutron fluence in 10^{24} n/m^3; T is the temperature in K; σ is the Mises stress in MPa, and ε depicts the true strain.

(2) The thermal creep behavior

The thermal creep rate model for Al 6061 is fitted according to the experimental data [29], expressed as [24]

$$\dot{\varepsilon}^{cr} = \begin{cases} 1.0 \times 10^{-8}[3.85105 + 3.81726 \times 10^{-6}\exp(0.0302T)]\sigma & \dot{\varepsilon}^{cr} < 1.0e-5 \\ 1.0 \times 10^{-8}(B\sigma + C) & \dot{\varepsilon}^{cr} \ge 1.0e-5 \end{cases} \tag{18}$$

where $\dot{\varepsilon}^{cr}$ denotes the creep strain rate in 1/h; σ is the Mises stress in MPa, and T is the temperature in K. The coefficients of A and B are related to the temperature, obtained as

$$\begin{cases} B = 1.34856 \times 10^{-2}(T - 273)^2 - 7.7364(T - 273) + 1.28196 \times 10^3 \\ C = -4.014(T - 273)^2 + 2.4732 \times 10^3(T - 273) - 3.6108 \times 10^5 \end{cases} \tag{19}$$

(3) The thermal expansion

The thermal expansion coefficient α in K^{-1} is expressed as [30]

$$\alpha(T) = (0.9T + 2018) \times 10^{-8} \tag{20}$$

(4) The thermal conductivity

The thermal conductivity k in W/(m K) is adopted as [30]

$$k(T) = -1.77 \times 10^{-4}T^2 + 0.19T + 138.55 \tag{21}$$

where T is the temperature in K.

2.2. Mesoscale normal stress

As shown in Fig. 1, the gas bubbles in the U-Mo fuel foil is assumed to obey a distribution pattern of FCC [31], Fig. 2 schematically illustrates the definitions for the macroscale and mesoscale normal stresses. The mesoscale stresses are related to the macroscale stresses, bubble pressure, surface tension and bubble size, expressed as [12]

$$\sigma_{meso} = \frac{\sigma_{macro} + 0.9596\phi^{2/3}\left(P - \frac{2\gamma_s}{r}\right)}{1 - 0.9596\phi^{2/3}} \tag{22}$$

where σ_{macro} refers to the first principal stress in the homogenized fuel foil, P is the equivalent bubble pressure; r denotes the equivalent bubble radius. The models of bubble pressure and bubble size can be found in Ref. [12].

The bubble volume fraction of ϕ is dependent on the irradiation swelling, expressed as [12]

$$\phi = \frac{SW_{gas}}{1 + SW_{gas} + SW_s} \tag{23}$$

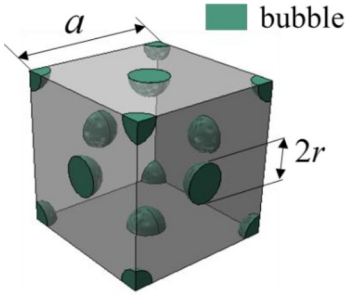

Fig. 1. Bubble arrangement in fuel foil [12].

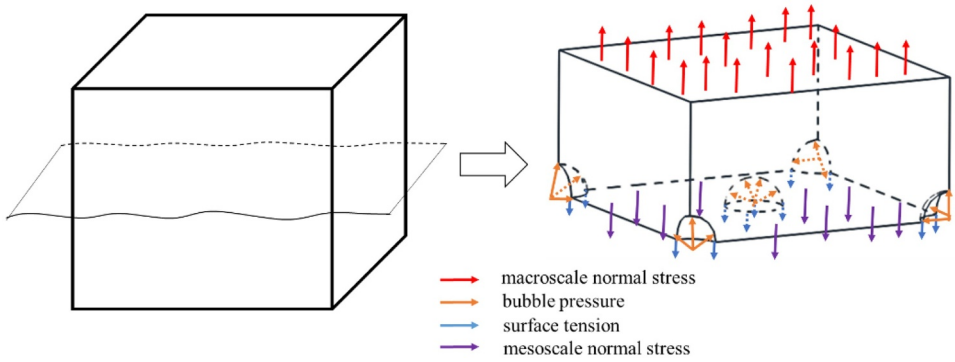

Fig. 2. The illustrations for definitions of the macroscale normal stress and mesoscale normal stress.

3. Finite element model

Five three-dimensional finite element models are built to implement the finite element simulations of in-pile thermo-mechanical behavior in monolithic U-Mo/Al fuel plates. In these models, only the irradiation creep model for the fuel foil is different. As given in Section 2.1.1, five creep coefficients of 10×10^{-31} m^3/MPa, 100×10^{-31} m^3/MPa, 500×10^{-31} m^3/MPa, 1000×10^{-31} m^3/MPa and 2000×10^{-31} m^3/MPa are adopted respectively, in order to investigate the effects of creep coefficient on the mesoscale mechanical behavior in the fuel foil during irradiation. The user-defined subroutines of UMATHT and UMAT are programmed to define the thermo-mechanical constitutive relations for the fuel foil and cladding in commercial software ABAQUS. The detailed three-dimensional stress update algorithm and consistent stiffness modulus can be found in Ref. [23]. It is noted that the fuel foil is set as a continuous media in the finite model, although it will evolve into a porous material with the fission gases in the bubbles. The macroscale stress in Eq. (13) can be firstly calculated. The models for bubble volume fraction, bubble pressure and bubble radius are involved in the finite element simulation. With their values substituted in Eq. (22), the mesoscale normal stress can be determined. Thus, the mesoscale mechanical behavior in the fuel foil can be obtained and analyzed. The flow chart for the calculation of mesoscale mechanical variables can be found in Ref. [12].

A RERTR-9A mini-plate L1P04A is taken into simulation, whose dimensions are $100 \times 25 \times 1.4$ mm with a fuel foil of $82.6 \times 19 \times 0.25$ mm. The distribution of fuel fission rate along the plate-width direction is plotted in Fig. 3 [20]. The fast neutron flux $\dot{\varphi}$ in n/(m^2 s) is also heterogeneous in plate-width direction. The total irradiation history is considered to be 98 days. Allowing for the symmetries in the structure and loading, 1/4 part of the whole fuel plate is chosen as the finite element model, as depicted in Fig. 4(a). The applied

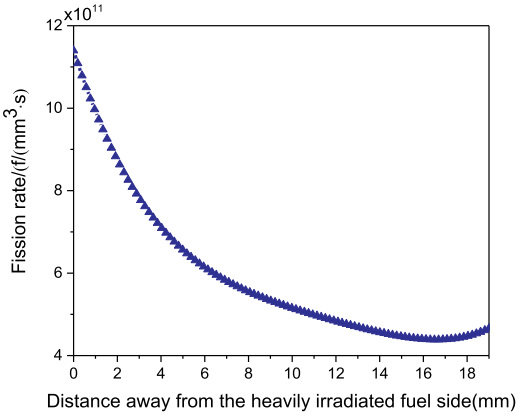

Fig. 3. The inhomogeneous fuel fission rate along the plate-width direction.

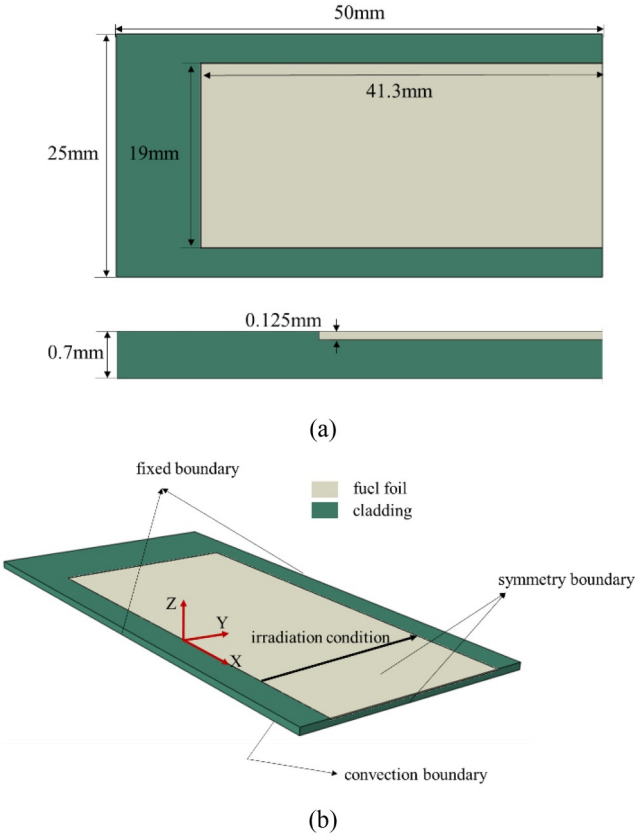

Fig. 4. (a) The finite element model and (b) the applied boundary conditions.

boundary conditions are shown in Fig. 4(b), together with the used coordinate system. In Fig. 5, the mesh grid and output path are given. The location-dependent fast neutron flux $\dot{\varphi}$ in n/(m^2·s) is expressed as

$$\dot{\varphi} = 3.24 \times 10^{17} \times (2.140 \times 10^{-4} y^4 - 1.003 \times 10^{-2} y^3 + 1.82 \times 10^{-1} y^2 - 1.651 y + 1.1398) \quad (24)$$

where the variable y represents the y-coordinate.

It is noted that the outer surface of the fuel plate maintains the convection boundary condition, where the temperature of coolant is 323 K and the heat transfer coefficient is 3.5×10^{-2} W/(mm^2·K), and the coolant pressure is zero.

4. Results and discussion

In this section, the deformation of fuel foil, the mesoscale normal

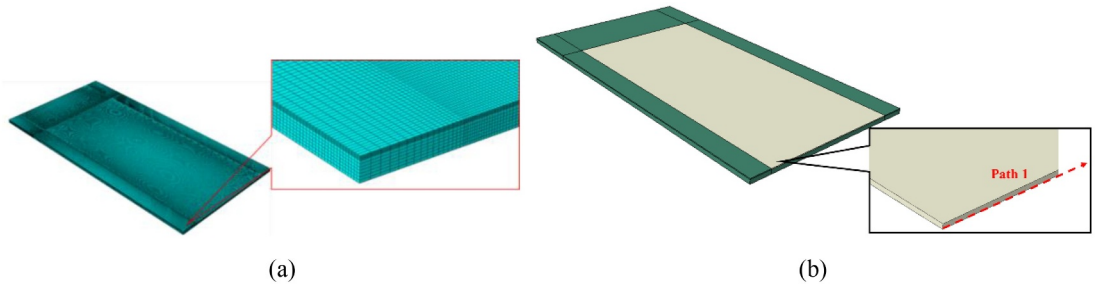

Fig. 5. (a) The mesh grid and (b) the output path.

stress, the bubble volume fraction, the bubble pressure and the through-thickness creep strain component for different cases of U-Mo irradiation creep coefficient are analyzed. The dangerous regions are predicted according to the mesoscale normal stresses and the through-thickness creep strain components. The suggestion for optimizing the U-Mo irradiation creep coefficient is proposed.

4.1. The fuel foil deformation

Fig. 6 presents the simulation results of thickness increment on the 98.0th day for U-Mo fuel foil with different creep coefficients, which are compared with the experimental data for the U-10Mo fuel foil at the same time. It can be observed that the simulation results for the creep coefficient of 2000×10^{-31} m^3/MPa are more close to the experimental data than the results for the other four creep coefficients. Thus, the creep coefficient of 2000×10^{-31} m^3/MPa can be identified for U-10Mo, which is much larger than 500×10^{-31} m^3/MPa obtained in Ref. [20]. In fact, one can see from Ref. [20] that the two-dimensional simulation results for a creep coefficient of 500×10^{-31} m^3/MPa can't match well with the experimental data. In Ref. [24], a creep coefficient of 1000×10^{-31} m^3/MPa for U-10Mo was identified when the thermal creep effect for the cladding was not considered; when the thermal creep was considered in the constitutive relation for the cladding, a creep coefficient of 2000×10^{-31} m^3/MPa for U-10Mo was also identified. In this study, the mechanistic model for fission gas swelling is considered, in which the external hydrostatic-pressure dependence is involved. For higher U-Mo creep coefficients, the external hydrostatic pressure approaches zero along Path 1. So, it is understandable that the same creep coefficient for U-10Mo can be identified whether the empirical model or mechanistic model for the fission gas swelling is used. Simultaneously, one can find that the maximum increment for the creep coefficient of 10×10^{-31} m^3/MPa is much lower than the results for the other creep coefficients, which results from the much higher external hydrostatic pressure occurred there. The distribution and evolution rules of thickness increments for the U-Mo fuel foil with different creep coefficient are similar to those in Ref. [24], which will not be described here.

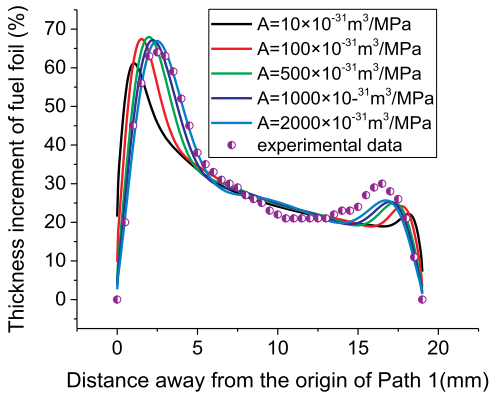

Fig. 6. The distributions of fuel foil thickness increments along Path 1 on the 98.0th day.

4.2. The mesoscale normal stress

It has been supposed that a tensile stress state in the fuel foil is a contributing factor for failure [32]. Meanwhile, the first principal stress is almost exactly parallel to the thickness direction [12,32], which is perpendicular to the fracture plane in the post-irradiation examination [4]. The mesoscale normal stress is calculated with the first principal stress according to Eq. (22), which is closely related to fuel fracture. Fig. 7 gives the contour plots of mesoscale normal stress in the fuel foil on the 98.0th day for five creep coefficients. It can be found that there are large mesoscale normal stresses in the fuel region close to the heavily irradiated edge for all the cases of different creep coefficients. The peak values are located near the corner. The effect of U-Mo creep coefficient on the mesoscale normal stress is noticeable. In the U-Mo creep coefficient range of 10×10^{-31} m^3/MPa to 1000×10^{-31} m^3/MPa, the maximum mesoscale normal stress decreases with the creep coefficient; in the fuel foil corners and edges, the mesoscale stresses will gradually turn into tensile stresses or smaller compressive stresses from extremely large compressive stresses. When the creep coefficient rises from 1000×10^{-31} m^3/MPa to 2000×10^{-31} m^3/MPa, the maximum mesoscale stress is heightened, and tensile stresses appear at a large area close to the heavily irradiated side, even at the fuel corner. One can conclude that the fuel foil with different irradiation creep coefficients will take on different fracture behavior, and an extremely large creep coefficient value should not be a good choice.

Fig. 8 gives the distributions of mesoscale normal stress and first principal stress along the paths in Fig. 7. It should be mentioned that those paths are close to the interface between the fuel foil and cladding. Fracture of the fuel foil near the interface was found in some post-irradiation examinations for U-Mo/Al monolithic fuel plates. It is clearly found from Fig. 8(a) that the positions of the peak mesoscale normal stress are close to the heavily irradiated edge. Except for the case with a creep coefficient of 2000×10^{-31} m^3/MPa, the distance of the peak stress away from the heavily irradiated side will increase with the U-Mo creep coefficient. The failure zone may be closer to the edge of fuel foil for a smaller U-Mo creep coefficient if fracture happens. When the irradiation creep coefficient increases from 10×10^{-31} m^3/MPa to 1000×10^{-31} m^3/MPa, the peak value of mesoscale normal stresses will decrease from 58.04 MPa to 28.04 MPa, with a reduction of ~52%.

The mesoscale normal stress is connected with the macroscale one. From Fig. 8(b), one can find that on the whole the region for tensile first principal stress expands with the decrease of creep coefficient. When the creep coefficient decreases from 1000×10^{-31} m^3/MPa to 10×10^{-31} m^3/MPa, the peak value of the first principal stress increases by 430%. The obtained results of first principal stress in the fuel foil are similar to those in Ref. [24] except for the creep coefficient case of 10×10^{-31} m^3/MPa, which relates to the different fission gas swelling models used in these two studies. In this study, the mechanistic model depending on the external hydrostatic pressure is adopted to result in smaller values for the creep coefficient of 10×10^{-31} m^3/MPa,

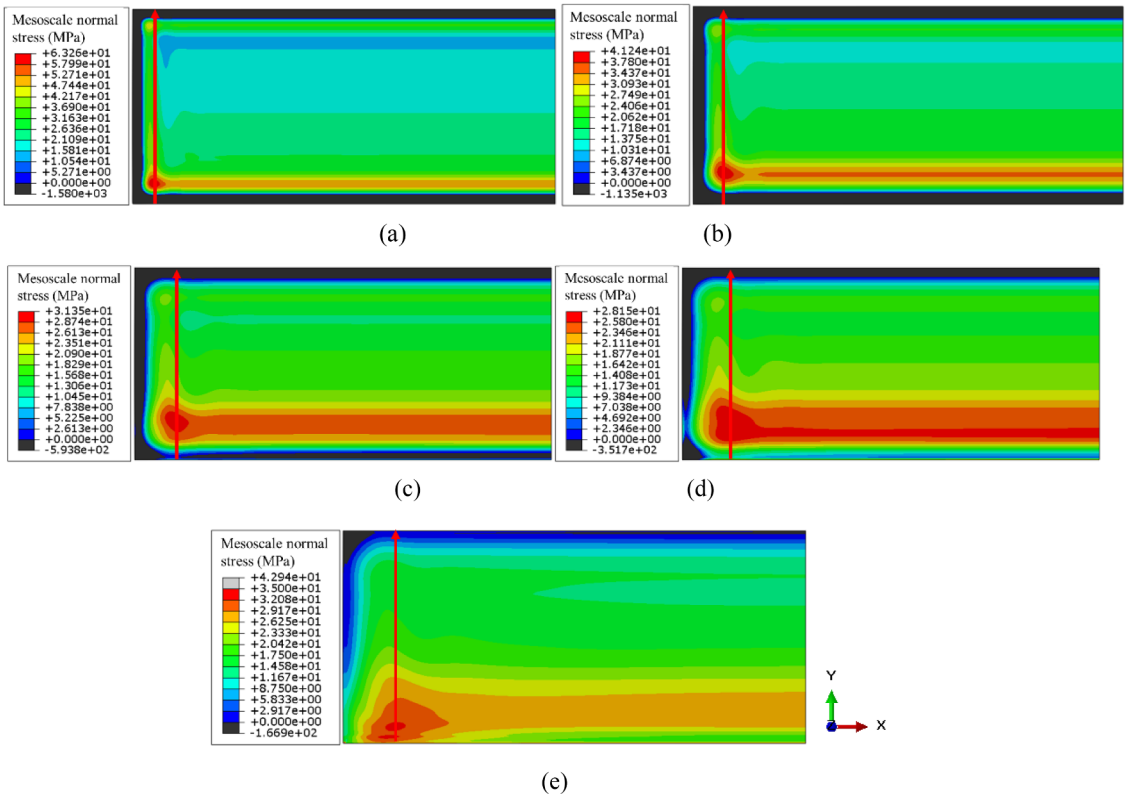

Fig. 7. The contour plots of mesoscale normal stress on 98.0th day when creep coefficient is (a) 10×10^{-31} m^3/MPa, (b) 100×10^{-31} m^3/MPa, (c) 500×10^{-31} m^3/MPa, (d) 1000×10^{-31} m^3/MPa and (e) 2000×10^{-31} m^3/MPa.

as mentioned in Section 4.1.

One can see that higher values of the first principal stress appear simultaneously near the heavily and weakly irradiated sides, and they are close to each other. Generally, the fuel foil will firstly break at the heavily irradiated region [4]. One can conclude that the dangerous regions in the fuel foil should not be determined only by the actual macroscale maximum tensile stresses because the ultimate macroscale strength will decrease with burnup [5], which is for the reason that the bubble volume fraction and bubble pressure will evolve with burnup Simultaneously, the ultimate strength of fuel skeleton may be weakened because of creep damage, similar to the other metals [9]. In Fig. 8(a), one can observe that the peak value of mesoscale tensile stress appears at the locations near the heavily irradiated side. It is noted that the dangerous points can't be judged only by the peak value of mesoscale normal stress. The distribution of through-thickness creep strain component (shown in Section 4.4) should be compared with that of mesoscale normal stress.

Comparing the stress results in Fig. 8(a) and (b), one can find that the peak values of mesoscale normal stress are much higher than those of the first principal stress, the peak values of mesoscale normal stress increase by 154%, 221%, 380% and 552% respectively for the U-Mo creep coefficients of 10×10^{-31} m^3/MPa, 100×10^{-31} m^3/MPa, 500×10^{-31} m^3/MPa and 1000×10^{-31} m^3/MPa. One can know from Eq. (22) that the obtained mesoscale normal stresses results from the contributions of bubble pressure, bubble volume fraction and bubble surface tension.

From Eq. (22), it can be found that both of the bubble volume fracture and bubble pressure tend to enlarge the mesoscale stress. However, the effect of surface tension on mesoscale stress is ambiguous, because its contribution is coupled with bubble size and bubble volume

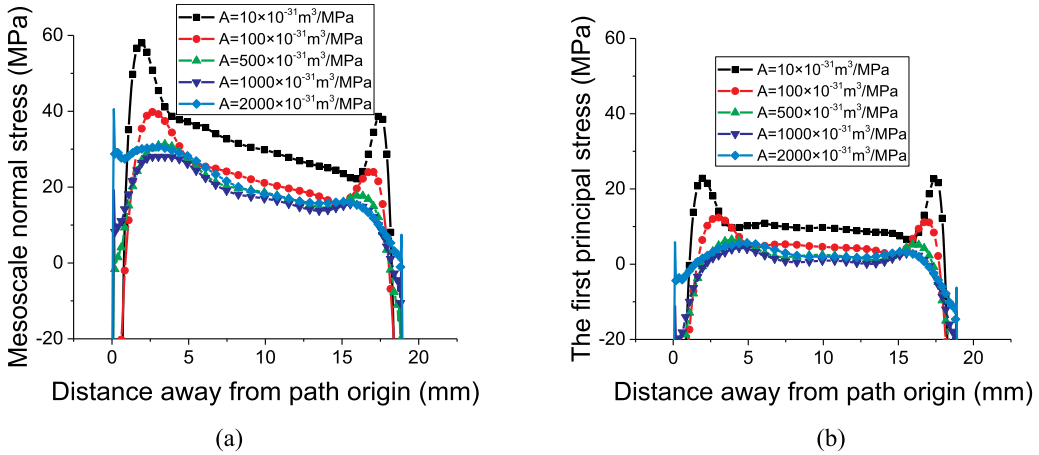

Fig. 8. The distributions of (a) mesoscale normal stress (b) the first principal stress on 98.0th day along the paths in Fig. 7.

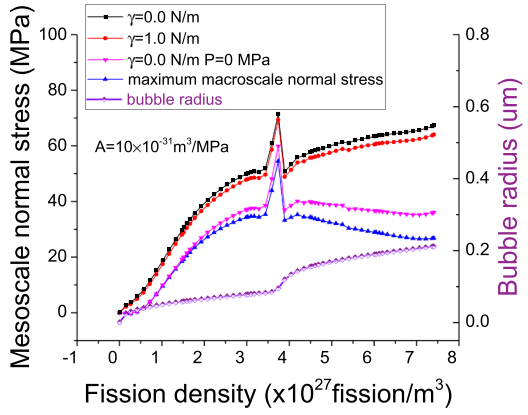

Fig. 9. The evolution results of stresses and bubble radius for the U-Mo creep coefficient of 10×10^{-31} m^3/MPa.

fraction [12]. Fig. 9 presents the evolution of maximum mesoscale normal stress with fission density under different assumptions when the U-Mo creep coefficient becomes 10×10^{-31} m^3/MPa. On the whole, the maximum mesoscale normal stress will rise with the fission density. A fluctuation can be found, which has relations with the grain recrystallization. Once the recrystallization starts, the local irradiation swelling is enhanced. The non-homogeneity of through-thickness deformation results in quick increase of tensile stress. With the progress of irradiation, recrystallization of the adjacent material occurs and leads to decrease of tensile stress.

It is clearly found from Fig. 9 that the surface tension has a slight impact on the mesoscale normal stress. The deviation of maximum mesoscale normal stresses with and without considering the surface tension maintains lower than 5%, which means that the contribution of surface tension in Eq. (22) can be ignored. It is known that at the initial stage of burnup, both of the bubble volume fraction and bubble radius are very small, the effect of bubble pressure dominates. With increase of bubble radius, the term of $2\gamma/r$ is much smaller than the bubble pressure [12], so the effect of surface tension isn't noticeable. In order to investigate the contribution of bubble pressure, Fig. 9 also gives the evolution results of maximum mesoscale normal stress with the bubble pressure in Eq. (22) set as zero. It can be found that the influence of bubble pressure on the mesoscale normal stress is remarkable. The mesoscale stress value on the 98.0th day without considering the contribution of bubble pressure is about 2/3 of the value with the bubble pressure taken into account. The effect of bubble pressure can't be neglected, especially when the bubble volume fraction is large.

4.3. The bubble volume fraction and bubble pressure

It can be obtained from Section 4.3 that the mesoscale normal stresses are greatly affected by the bubble volume fraction and bubble pressure. Fig. 10 displays the contour plots of bubble volume fraction of fuel foil on the 98.0th day. It can be found that the bubble volume fractions are higher at the region near the heavily irradiated side, and their values there vary with the U-Mo creep coefficients. The maximum bubble volume fraction increases with the U-Mo creep coefficient. With the U-Mo creep coefficient raised from 10×10^{-31} m^3/MPa to 2000×10^{-31} m^3/MPa, the maximum value of bubble volume fraction increase by ~21%. Fig. 11 exhibits the distributions of bubble volume fraction along the paths in Fig. 7. One can observe that the positions of peak value of bubble volume fraction are different for five U-Mo creep coefficients. It can be seen that the maximum bubble volume fraction appears very close to the heavily irradiated side for the creep coefficients of 2000×10^{-31} m^3/MPa, 1000×10^{-31} m^3/MPa and 500×10^{-31} m^3/MPa. For the rest cases, the positions of the peak values have a certain distance away from the path origin, and the distance is larger for the creep coefficient of 100×10^{-31} m^3/MPa. In the major part of the path, the volume fractions are similar for the creep coefficients excluding 10×10^{-31} m^3/MPa. For the creep coefficient of 10×10^{-31} m^3/MPa, the bubble volume fraction is the smallest.

The bubble volume fraction depends on the fission gas swelling influenced by the external hydrostatic pressure. Higher external hydrostatic pressures induce smaller fission gas swelling together with lower bubble volume fraction. From Fig. 11(b), one can see that there are larger hydrostatic pressures at both sides of the fuel foil for all creep coefficients. For the creep coefficient of 10×10^{-31} m^3/MPa, the hydrostatic pressure is the largest at the whole path, so the bubble volume fraction is the smallest. The external hydrostatic pressures in the middle part of the paths are close to zero for the creep coefficients excluding 10×10^{-31} m^3/MPa. So, the results in Fig. 11(a) can be understandable.

Fig. 12 depicts the distributions of bubble pressure for five different creep rate coefficients. One can find that around the two ends of the paths the bubble pressures for different creep coefficients differ from each other greatly. The bubble pressures at the two ends increase with a decrease of the creep coefficient, which is consistent with the results of bubble volume fraction in Fig. 11(a). The bubble radii at the two ends are much smaller than those at the other regions, so the bubble pressures are the highest there.

4.4. The through-thickness creep strain components

As mentioned in Section 4.2, the dangerous regions in the fuel foil should be determined not only by the mesoscale normal stresses, but also the degraded ultimate strength of skeleton materials due to creep damage. In general, the through-thickness (parallel to the direction of mesoscale normal stress) creep strain component of ε_{33}^{cr} is used to characterize the creep damage in metal materials [33]. Only positive values of creep strain component of ε_{33}^{cr} will induce creep damage to reduce the strength of materials [32]. Fig. 13 gives the contour plots of ε_{33}^{cr} on the 98.0th day for the fuel foil. It can be found that as the irradiation creep coefficient increases, ε_{33}^{cr} rises greatly. Particularly, when the creep coefficient exceeds 500×10^{-31} m^3/MPa, the maximum value of ε_{33}^{cr} can become ~3 times of the one for the creep coefficient of 10×10^{-31} m^3/MPa. In Fig. 14, the evolutions of ε_{33}^{cr} with the fission density are depicted for different creep coefficients. It is noted that the outputted creep strain components in Fig. 14 refer to the peak values along the paths in Fig. 7, where larger mesoscale normal stresses locate. Due to that the points with the maximum creep strain components for different creep coefficients situate at varied locations, so the reached fission density differs from each other at certain irradiation time. It can be observed that the creep strain components all increse with burnup. Excluding the creep coefficient case of 2000×10^{-31} m^3/MPa, the creep strain components increase slowly with the fission density although the values for larger creep coefficients appear higher. For the creep coefficient of 2000×10^{-31} m^3/MPa, the creep strain components at higher fission densities increase sharply.

Considering that the creep strain component impacts the strength of fuel foil skeleton, it should combine the creep strain component and mesoscale normal stress to judge the dangerous regions. Fig. 15 gives the distributions of through-thickness creep strain and mesoscale normal stress on the 98.0th day along the paths in Fig. 7. It can be found that the location with the maximum mesoscale normal stress doesn't have the peak value of creep strain component for all the creep coefficients. Larger creep strain components exist in the left of the maximum mesoscale normal stress point, so the dangeous points are possible to appear in these regions although the mesoscale normal stresses becomes lower. The dangerous regions are indicated in Fig. 15. So, it means that the initial failure may happen more close to the egdes of fuel foil with increasing burnup. This is consistent with the fact that the fracture or blister phenomenon is usually observed colse to the edge of fuel foil in some monolithic fuel plates [4].

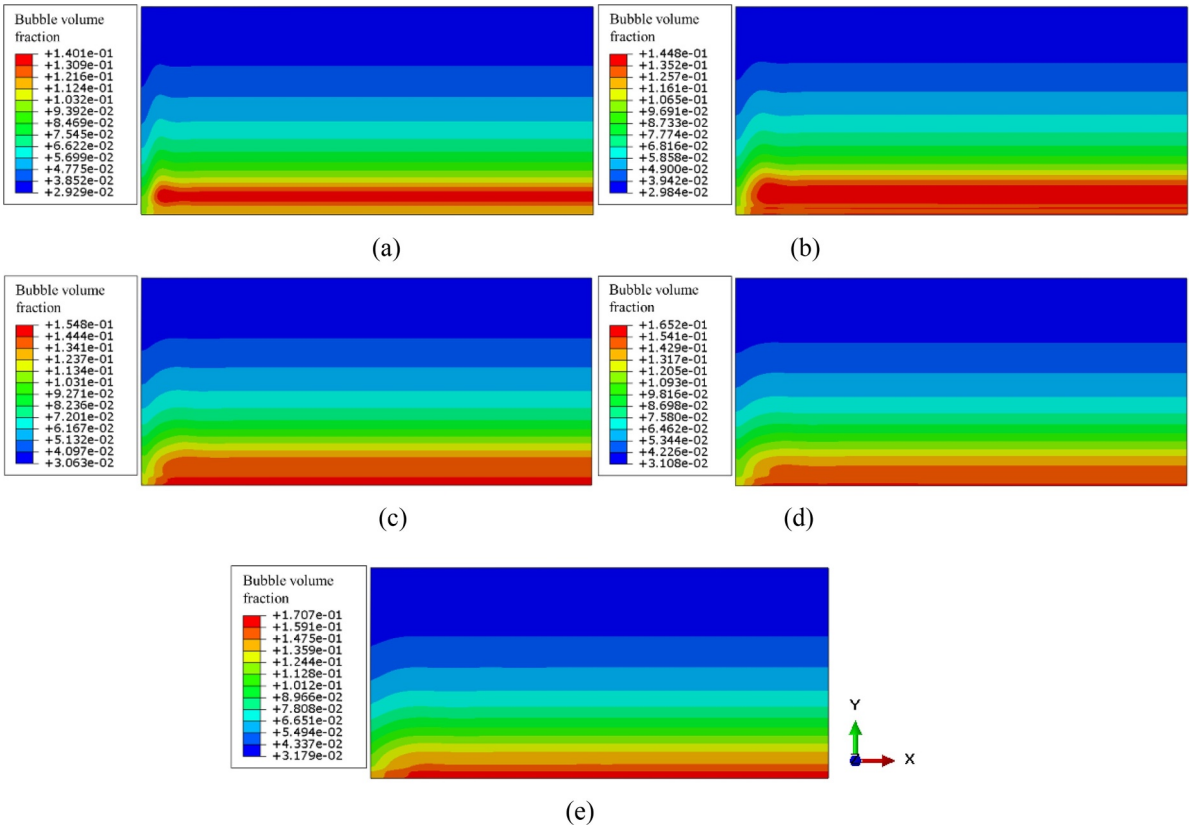

Fig. 10. The contour plots of bubble volume fraction on 98.0th day when creep coefficient is (a) 10×10^{-31} m^3/MPa, (b) 100×10^{-31} m^3/MPa, (c) 500×10^{-31} m^3/MPa, (d) 1000×10^{-31} m^3/MPa and (e) 2000×10^{-31} m^3/MPa.

The irradiation creep performance should be optimized, because the creep-induced damage tends to degrade the mesoscale strength of the fuel foil. A small amount of oxygen can reduce the creep strain of tungsten significantly [34], and the creep rate of U-Nb-Zr alloys will decrease drastically with the increase of Nb content [22], so it can be deduced that addition of some other trace elements into the current U-10Mo may considerably change the creep coefficient. Fig. 16 gives the distribution of mesoscale normal stress and corresponding through-thickness creep strain components for different creep coefficients. The through-thickness creep strain components increase by ~5% when the creep coefficient increases from 10×10^{-31} m^3/MPa to 1000×10^{-31} m^3/MPa, and the mesoscale stresses decreases by ~52%. With an increase of irradiation creep coefficient from 1000×10^{-31} m^3/MPa to 2000×10^{-31} m^3/MPa, the effective mesoscale normal stresses increase by ~9%, and the through-thickness creep strain components increase by ~219%. It is clearly found that those creep strain components are much lower for the creep coefficients excluding 2000×10^{-31} m^3/MPa. When creep coefficient increases from 1000×10^{-31} m^3/MPa to 2000×10^{-31} m^3/MPa, the creep strain component has an increase of ~2 times; and the mesoscale tensile stress also rises. One can conclude that an extreme large creep coefficient is not a good choice, and the irradiation creep performance for U-Mo fuels should be optimized.

If the creep coefficient is different, the strength of fuel foil may have some differences, and the creep damage model to define the relations of the degradated strength with the irradiation creep strain component may be discrepant. However, no studies can be found in the literatures that have dealt with the irradiated tensile strength considering the

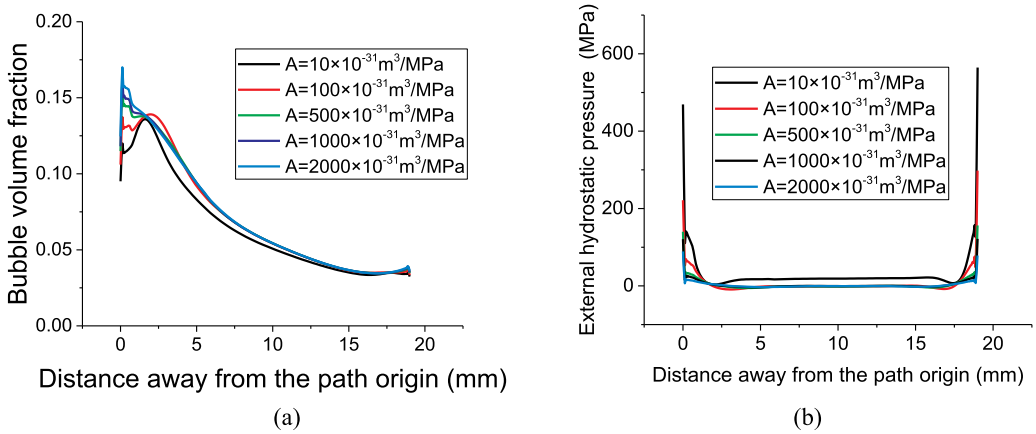

Fig. 11. The distributions of (a) bubble volume fraction (b) external hydrostatic pressure on the 98.0th day along the paths in Fig. 7.

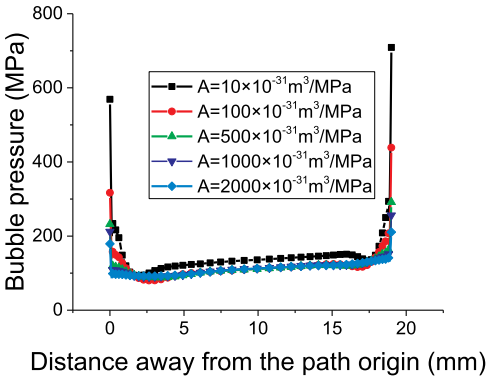

Fig. 12. The distribution of bubble pressure on the 98.0th day along the paths in Fig. 7.

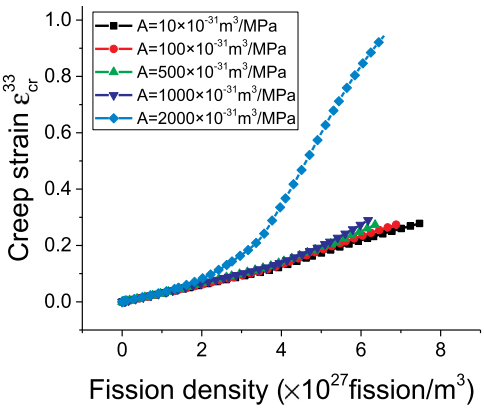

Fig. 14. The evolutions of creep strain with different creep rate coefficient.

creep damage at present, the creep damage model for U-Mo fuel foils is ambigious. So, the competition between maximum mesoscale normal stress and creep damage is indefinite. To precisely predict the lifetime of U-Mo fuels, the mesoscale strength model dependent on the creep strain component should be developed further.

5. Conclusion

In this study, three dimensional finite element simulations for the thermo-mechanical coupling behavior in different U-Mo/Al monolithic fuel plates are implemented, with the irradiation creep coefficients increasing from 10×10^{-31} m^3/MPa to 2000×10^{-31} m^3/MPa, in which the mechanistic fission gas swelling model dependent on external hydrostatic pressure is adopted. The variables of through-thickness deformation and creep strain component, the bubble volume fraction, bubble pressure and mesoscale normal stress are analyzed for the fuel foil with different creep coefficients. The main conclusions can be drawn as follows:

(1) The creep coefficient of U-10Mo is recognized as 2000×10^{-31} m^3/MPa, because the simulation results of thickness increment are in good agreement with the measureable data.
(2) The maximum bubble volume fraction in the fuel foil increases with the creep coefficient, with the maximum value on the 98.0th day raised by ~21% when the creep coefficient increases from 10×10^{-31} m^3/MPa to 2000×10^{-31} m^3/MPa.
(3) The maximum mesoscale normal stress in the fuel foil decreases with the creep coefficient on the whole, and the effect of surface tension on the mesoscale normal stress can be negligible. The peak value can reach 63 MPa on the 98.0th day for the creep coefficient of 10×10^{-31} m^3/MPa, which is 2.25 times of the value for the

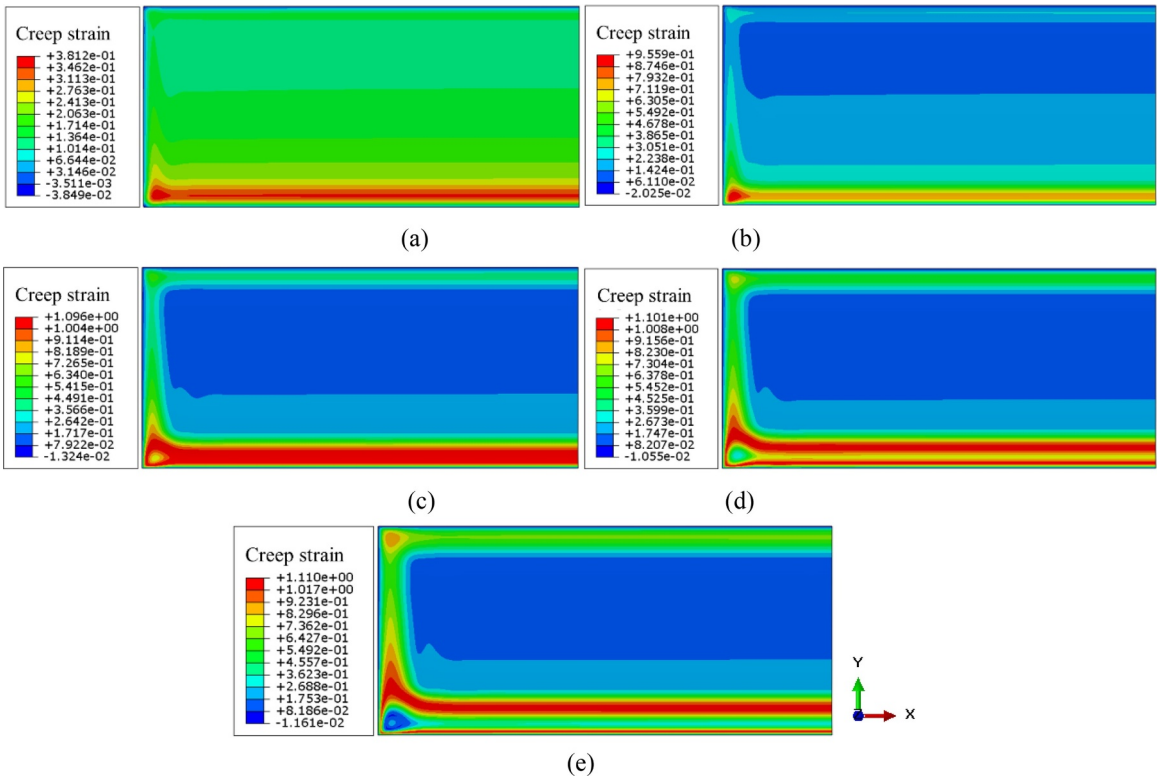

Fig. 13. The contour plots of creep strain component ε_{33}^{cr} of fuel foil on 98.0th day when creep coefficient is (a) 10×10^{-31} m^3/MPa, (b) 100×10^{-31} m^3/MPa, (c) 500×10^{-31} m^3/MPa, (d) 1000×10^{-31} m^3/MPa and (e) 2000×10^{-31} m^3/MPa.

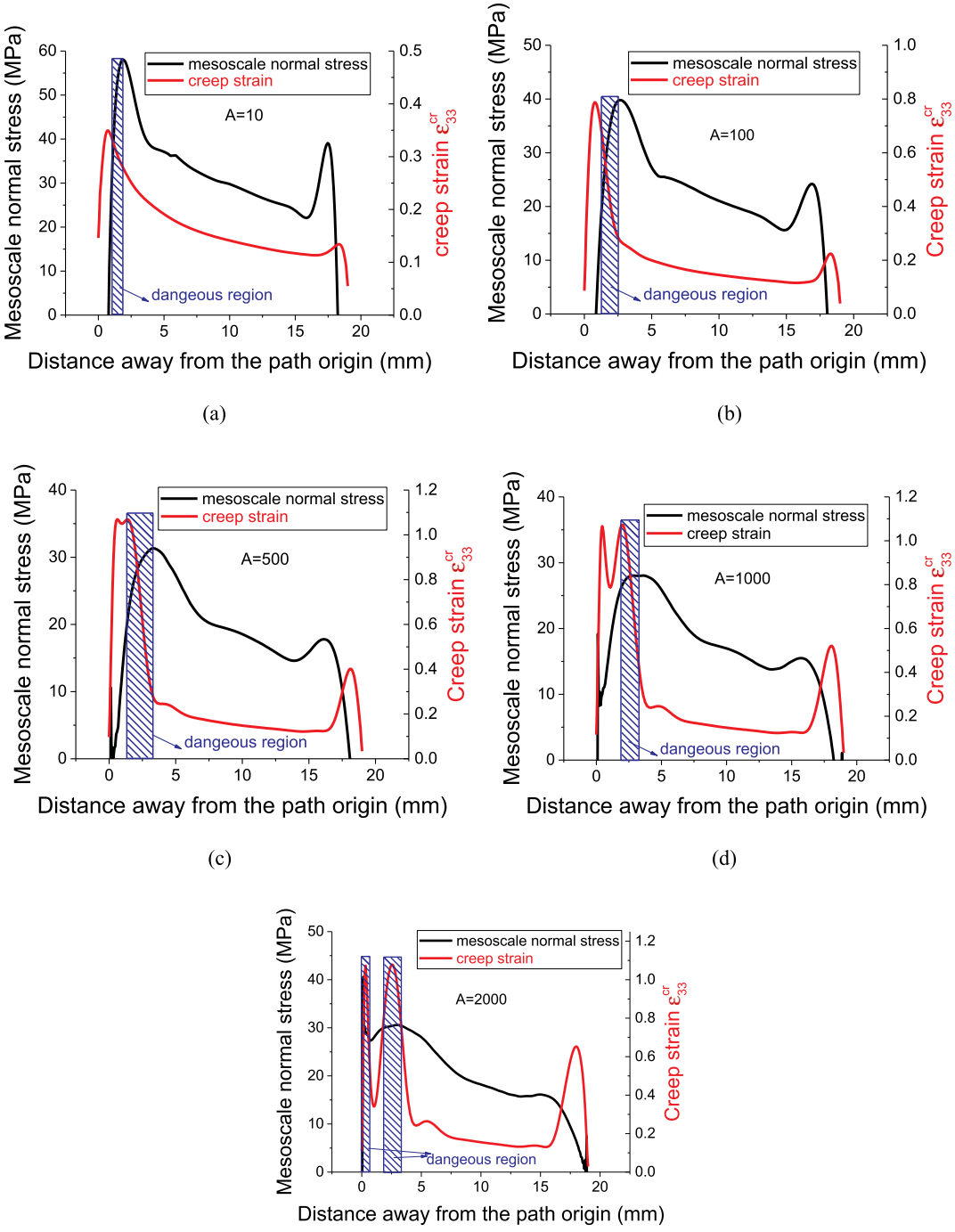

Fig. 15. The distribution of creep strain and mesoscale normal stress along the paths in Fig. 7 for the creep coefficients of (a) 10×10^{-31} m^3/MPa (b) 100×10^{-31} m^3/MPa (c) 500×10^{-31} m^3/MPa (d) 1000×10^{-31} m^3/MPa (e) 2000×10^{-31} m^3/MPa.

creep coefficient of 1000×10^{-31} m^3/MPa.

(4) The dangerous region of fuel foil is surrounding the points with the maximum mesoscale normal stress.

(5) When the irradiation creep coefficient increases from 10×10^{-31} m^3/MPa to 1000×10^{-31} m^3/MPa, the maximum mesoscale normal stresses will decrease from 58.04 MPa to 28.04 MPa, with a reduction of ~52%; while the through-thickness creep strain components increase by ~5%. With an increase of irradiation creep coefficient from 1000×10^{-31} m^3/MPa to 2000×10^{-31} m^3/MPa, the maximum mesoscale normal stresses increase by ~9%, and the through-thickness creep strain components increase by ~219%. For the sake of U-Mo fuel integrity, an extreme large creep coefficient is not a good choice, and the irradiation creep performance needs to be optimized.

Declaration of Competing Interest

The authors declared that we have no conflicts of interest to this work.

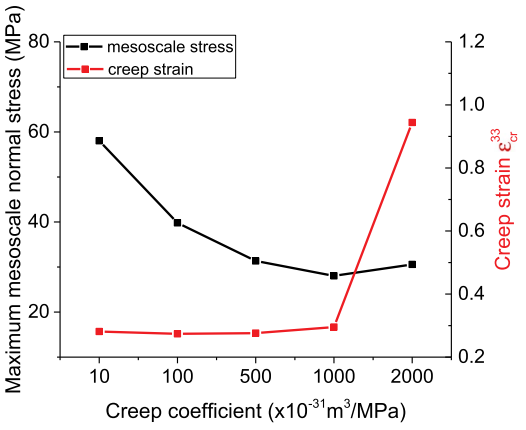

Fig. 16. The distribution of maximum mesoscale normal stress and corresponding creep strain components for different creep coefficients.

Acknowledgments

The authors thank for the supports of National Natural Science Foundation of China (Nos. 11572091, 11772095) and the support of the National Key Research and Development Program of China (2016YFB0700103), the supports of the foundation from Science and Technology on Reactor System Design Technology Laboratory.

References

[1] D.B. Lee, K.H. Kim, C.K. Kim, Thermal compatibility studies of unirradiated U·Mo alloys dispersed in aluminum, J. Nucl. Mater. 250 (1997) 79–82.
[2] M.K. Meyer, G.L. Hofman, S.L. Hayes, et al., Low-temperature irradiation behavior of uranium–molybdenum alloy dispersion fuel, J. Nucl. Mater. 304 (2002) 221–236.
[3] J. Park, K. Kim, C. Kim, et al., The irradiation behavior of atomized U-Mo alloy fuels at high temperature, Met. Mater. Int. 7 (2001) 151–157.
[4] M.K. Meyer, J. Gan, J.F. Jue, et al., Irradiation performance of U-Mo monolithic fuel, Nucl. Eng. Technol. 46 (2014) 169–182.
[5] J.L. Schulthess, W.R. Lloyd, B. Rabin, et al., Mechanical properties of irradiated U-Mo alloy fuel, J. Nucl. Mater. 515 (2019) 91–106.
[6] S. Hu, A.M. Casella, C.A. Lavender, et al., Assessment of effective thermal conductivity in U–Mo metallic fuels with distributed gas bubbles, J. Nucl. Mater. 462 (2015) 64–76.
[7] D.E. Burkes, A.M. Casella, A.J. Casella, et al., Thermal properties of U–Mo alloys irradiated to moderate burnup and power, J. Nucl. Mater. 464 (2015) 331–341.
[8] G.Y. Jeong, Y.S. Kim, Y.J. Jeong, et al., Development of prime for irradiation performance analysis of U-Mo/Al dispersion fuel, J. Nucl. Mater. 502 (2018) 331–348.
[9] Q. Meng, Z. Wang, Creep damage models and their applications for crack growth analysis in pipes: a review, Eng. Fract. Mech. 205 (2019) 547–576.
[10] X. Du, Z. Jie, L. Yinghua, Plastic failure analysis of defective pipes with creep damage under multi-loading systems, Int. J. Mech. Sci. 128-129 (2017) 428–444.
[11] J.F. Mao, J.W. Zhu, S.Y. Bao, et al., Creep deformation and damage behavior of reactor pressure vessel under core meltdown scenario, Int. J. Press. Vessels Pip. 139-140 (2016) 107–116.
[12] X. Jian, X. Kong, S. Ding, A mesoscale stress model for irradiated U-10Mo monolithic fuels based on evolution of volume fraction/radius/internal pressure of bubbles, Nucl. Eng. Technol. 51 (2019) 1575–1588.
[13] J. Jue, D.D. Keiser, B.D. Miller, et al., Effects of irradiation on the interface between U-Mo and zirconium diffusion barrier, J. Nucl. Mater. 499 (2018) 567–581.
[14] A.M. Casella, D.E. Burkes, P.J. MacFarlan, et al., Characterization of fission gas bubbles in irradiated U-10Mo fuel, Mater. Charact. 131 (2017) 459–471.
[15] Y.S. Kim, G.L. Hofman, Fission product induced swelling of U–Mo alloy fuel, J. Nucl. Mater. 419 (2011) 291–301.
[16] J. Rest, A model for the effect of the progression of irradiation-induced recrystallization from initiation to completion on swelling of UO2 and U–10Mo nuclear fuels, J. Nucl. Mater. 346 (2005) 226–232.
[17] J. Rest, A model for the influence of microstructure, precipitate pinning and fission gas behavior on irradiation-induced recrystallization of nuclear fuels, J. Nucl. Mater. 326 (2004) 175–184.
[18] Y. Cui, S. Ding, Z. Chen, et al., Modifications and applications of the mechanistic gaseous swelling model for UMo fuel, J. Nucl. Mater. 457 (2015) 157–164.
[19] W. Dienst, Irradiation induced creep of ceramic nuclear fuels, J. Nucl. Mater. 65 (1977) 1–8.
[20] Y.S. Kim, G.L. Hofman, J.S. Cheon, et al., Fission induced swelling and creep of U–Mo alloy fuel, J. Nucl. Mater. 437 (2013) 37–46.
[21] T.R.G. Kutty, S. Kaity, A. Kumar, Impression creep behaviour of U − 6%Zr alloy: role of microstructure, Procedia Eng. 55 (2013) 561–565.
[22] K. Ghoshal, T.R.G. Kutty, S. Mishra, et al., Creep studies on U–7%Zr, U–7%Nb and U rich U–Nb–Zr alloys, J. Nucl. Mater. 432 (2013) 20–22.
[23] X. Kong, X. Tian, F. Yan, et al., Thermo-mechanical behavior simulation coupled with the hydrostatic-pressure-dependent grain-scale fission gas swelling calculation for a monolithic UMo fuel plate under heterogeneous neutron irradiation, Open Eng. 8 (2018) 243–260.
[24] F. Yan, J. Xiaobin, D. Shurong, Effects of UMo irradiation creep on the thermo-mechanical behavior in monolithic UMo/Al fuel plates, J. Nucl. Mater. 524 (2019) 209–217.
[25] N. Ramakrishnan, V.S. Arunachalam, Effective elastic moduli of porous solids, J. Mater. Sci. 25 (1990) 3930–3937.
[26] J. Rest, Y.S. Kim, G.L. Hofman, et al., U-Mo Fuels Handbook. Argonne National Laboratory Report ANL-09/31, Chicago, Illinois, (2009).
[27] J. Jue, D.D. Keiser, C.R. Breckenridge, et al., Microstructural characteristics of HIP-bonded monolithic nuclear fuels with a diffusion barrier, J. Nucl. Mater. 448 (2014) 250–258.
[28] J. Spino, J. Rest, W. Goll, et al., Matrix swelling rate and cavity volume balance of UO2 fuels at high burn-up, J. Nucl. Mater. 346 (2005) 131–144.
[29] M.F. Marchbanks, ANS Materials Data Book, Oak Ridge National Laboratory, 1995.
[30] H. Ozaltun, M.H. Herman Shen, P. Medvedev, Assessment of residual stresses on U10Mo alloy based monolithic mini-plates during Hot Isostatic Pressing, J. Nucl. Mater. 419 (2011) 76–84.
[31] S. Hu, W. Setyawan, V.V. Joshi, et al., Atomistic simulations of thermodynamic properties of Xe gas bubbles in U10Mo fuels, J. Nucl. Mater. 490 (2017) 49–58.
[32] S.J. Miller, H. Ozaltun, Evaluation of U10Mo fuel plate irradiation behavior via numerical and experimental benchmarking, Proceedings of the ASME 2012 International Mechanical Engineering Congress & Exposition IMECE2012 November 9-15, Houston, Texas, USA, 2012.
[33] J. Hu, T. Fukahori, T. Igari, et al., Modelling of creep rupture of ferritic/austenitic dissimilar weld interfaces under mode I fracture, Eng. Fract. Mech. 191 (2018) 344–364.
[34] J. Webb, S. Gollapudi, I. Charit, An overview of creep in tungsten and its alloys, Int. J. Refract. Met. Hard. Mater. (2019).